ENVIRONMENTAL RESEARCH
LETTERS

LETTER • OPEN ACCESS

Quality and sensitivity of high-resolution numerical simulation of urban heat islands

To cite this article: Dan Li and Elie Bou-Zeid 2014 *Environ. Res. Lett.* **9** 055001

OPEN ACCESS
IOP Publishing
Environmental Research Letters
Environ. Res. Lett. **9** (2014) 055001 (14pp)
doi:10.1088/1748-9326/9/5/055001

Quality and sensitivity of high-resolution numerical simulation of urban heat islands

Dan Li[1] **and Elie Bou-Zeid**

Department of Civil and Environmental Engineering, Princeton University, Princeton, NJ, 08540, USA

E-mail: danl@princeton.edu

Received 16 January 2014, revised 19 March 2014
Accepted for publication 31 March 2014
Published 2 May 2014

Abstract

High-resolution numerical simulations of the urban heat island (UHI) effect with the widely-used Weather Research and Forecasting (WRF) model are assessed. Both the sensitivity of the results to the simulation setup, and the quality of the simulated fields as representations of the real world, are investigated. Results indicate that the WRF-simulated surface temperatures are more sensitive to the planetary boundary layer (PBL) scheme choice during nighttime, and more sensitive to the surface thermal roughness length parameterization during daytime. The urban surface temperatures simulated by WRF are also highly sensitive to the urban canopy model (UCM) used. The implementation in this study of an improved UCM (the Princeton UCM or PUCM) that allows the simulation of heterogeneous urban facets and of key hydrological processes, together with the so-called CZ09 parameterization for the thermal roughness length, significantly reduce the bias (<1.5 °C) in the surface temperature fields as compared to satellite observations during daytime. The boundary layer potential temperature profiles are captured by WRF reasonable well at both urban and rural sites; the biases in these profiles relative to aircraft-mounted senor measurements are on the order of 1.5 °C. Changing UCMs and PBL schemes does not alter the performance of WRF in reproducing bulk boundary layer temperature profiles significantly. The results illustrate the wide range of urban environmental conditions that various configurations of WRF can produce, and the significant biases that should be assessed before inferences are made based on WRF outputs. The optimal set-up of WRF-PUCM developed in this paper also paves the way for a confident exploration of the city-scale impacts of UHI mitigation strategies in the companion paper (Li *et al* 2014).

Keywords: urban canopy model, urban heat island, thermal roughness length, WRF

1. Introduction

The 'urban heat island' (UHI) is probably the most well-known environmental impact of urbanization (Oke 1982), and the most well-documented example of anthropogenic climate modification through land use change (Arnfield 2003). It arises from a variety of factors: the extensive use of man-made materials that have substantially different thermal and hydrological properties compared to natural materials, the reduction of evapotranspiration due to limited water bodies and green surfaces, and the anthropogenic heat sources (Grimmond 2007; Oke 1982), to name a few. Recent years have witnessed a growing interest from the scientific community, the public, and policy makers in understanding and mitigating UHIs, particularly due to the added pressure of increasing global urbanization and climate change. Currently, over 50% of the world population is living in cities, and this percentage continues to rise rapidly. By 2030, the urban population is expected to exceed 60% of the global population; 95% of the net future increase in the global population will occur in cities (Grimm *et al* 2008). The combined effects of UHIs, global climate change, and soaring urban populations pose significant challenges to energy and water sustainability and to human health in urban environments. In

[1] Now in the Program of Atmospheric and Oceanic Sciences, Princeton University, Princeton, NJ, 08540, USA and the NOAA/Geophysical Fluid Dynamics Laboratory, Princeton, NJ, 08540, USA.

particular, a recent study has shown that heat waves, which are projected to become more frequent and last longer under a warming climate (Lau and Nath 2012; Meehl and Tebaldi 2004), interact nonlinearly with UHIs to produce extremely high heat stress for urban residents (Li and Bou-Zeid 2013).

The scientific research on UHIs has traditionally focused on their energetic basis and characteristics (see e.g., Christen and Vogt 2004; Cleugh and Oke 1986; Dabberdt and Davis 1978; Grimmond *et al* 1993; Grimmond and Oke 1995 1999; Loridan and Grimmond 2012; Oke 1982; Oke *et al* 1999; Peterson and Stoffel 1980; Ryu and Baik 2012), as well as on their impacts on regional hydrometeorology and climate (e.g. Bornstein and Lin 2000; Dixon and Mote 2003; Li *et al* 2013a; Miao *et al* 2011; Shephard 2005; Zhang *et al* 2009). More recently, high-resolution numerical simulations of UHIs under real atmospheric conditions are increasingly being used to investigate the dynamics of these events and their potential mitigation (see e.g., Grossman-Clarke *et al* 2010; Li and Bou-Zeid 2013), partly due to the urgency of providing a decision framework for policy makers (Chow *et al* 2012). However, the capability of high-resolution numerical models to faithfully capture all the spatial and temporal dynamics of UHIs is far from being a settled matter. Two related open questions are: what aspects of a numerical model are most critical to the simulated UHI and can model-improvements focusing on these aspects improve the quality and reliability of UHI simulations?

This study aims to assess the quality and sensitivity of UHI simulations, and to improve them by coupling a new-generation urban canopy model (the Princeton UCM or PUCM) with a regional climate model, the Weather Research and Forecasting model (WRF). The sensitivity of the model's performance to the choice of physical parameterizations in WRF is investigated based on high-resolution simulations over the Baltimore–Washington metropolitan area. The new UCM is a simple, yet more realistic, representation of urban environments and surface energy budgets compared to the default UCM in WRF. More importantly, it allows the investigation of realistic mitigation strategies such as the use of green roofs and white roofs (Wang *et al* 2013), which are the focus of the companion paper of this study (Li *et al* 2014).

The scenario that we selected to study is the hottest day during a heat wave period that has been investigated previously by the authors (Li and Bou-Zeid 2013). A heat wave is recognized as a sustained period (longer than 72 h) during which the temperatures (usually the daily maximum temperatures or the nighttime minimum temperatures) exceed a certain threshold percentile (95th or 97.5th for example) of the climatic temperature distributions (Robinson 2001; Meehl and Tebaldi 2004; Lau and Nath 2012). Due to the UHI effect, cities are already hotter than rural areas (Grimmond 2007). Heat waves worsen the conditions in urban areas not only by boosting the temperature of both urban and rural areas, but also because urban temperatures are increased more intensely than rural temperatures during heat waves (Li and Bou-Zeid 2013). Under such conditions, mitigation strategies are critically needed to reduce the health risks in urban areas.

The paper is organized as follows: section 2 presents the WRF set up and experimental data sets; section 3 presents the findings and results. Section 4 concludes the study and discusses its implications.

2. Methodology

2.1. WRF model description and setup

In this study, the WRF version 3.3 is used. WRF is a non-hydrostatic, mesoscale numerical weather prediction model that solves the conservation equations of mass, momentum and energy on terrain-following coordinates (Skamarock and Klemp 2008). It has multiple parameterization schemes for each of its five physical packages: cumulus clouds, microphysics, radiation, planetary boundary layer (PBL), and surface (Skamarock and Klemp 2008). WRF has been widely used to study urban meteorology (see Chen *et al* 2011 for a review). This is largely attributable to the nesting capability of WRF that allows high-resolution simulations, and to the UCMs coupled into the WRF that allow a better representation of complex urban environments. For example, the default single-layer UCM that is coupled with the Noah land surface model in WRF can represent three types of urban facets: roof, wall and ground. In addition, the WRF–UCM framework can distinguish between three urban categories: low density residential, high density residential, and industrial/commercial.

The UCM has been shown to be critical for reproducing the correct air/surface temperature patterns in the urban areas (Lee *et al* 2011; Li and Bou-Zeid 2013; Zhang *et al* 2011). Although the default single-layer UCM can include three types of urban facets, it represents these urban facets as homogeneous surfaces and thus cannot simulate fractional white (high-reflectivity) roof coverage for example. These homogeneous surfaces are also impervious and are assumed not to contribute to evapotranspiration except when rainfall occurs (they have zero surface water storage capacity). As such, an improved UCM was implemented into WRF (hereafter PUCM due to its development at Princeton University as an offline urban model). There are many advantages of PUCM over the default UCM such as its ability to simulate heterogeneous facets, with subfacets consisting of different materials. For example, roof surface can be a combination of conventional roofs and green/white roofs; ground surface can be a combination of asphalt, concrete, and urban grass. For realistic representation of these green roofs and urban grass in PUCM, detailed models of hydrologic processes in the urban canyon were included. Realistic water storage and flux representation was shown to be crucial to the performance of urban models (Grimmond *et al* 2010, 2011). In addition, the use of urban material properties calibrated for the northeastern United States makes PUCM a particularly powerful tool for diagnosing UHI effects and mitigation in that region. The full details and validation of the new UCM, and the material properties calibration, can be found in Wang *et al* (2011a, 2011b, 2013); note however that some aspects of the offline PUCM, such as analytical solution of the heat

conduction equation and the independent treatment of in-canyon grass that are detailed and tested in Wang *et al* (2011a, 2011b, 2013), were not implemented in WRF since their impact on the analyses we perform here is deemed minor. The offline PUCM allows a detailed analysis of the building-scale impact of mitigation strategies such as the use of green roof and white roof (Wang *et al* 2013, see also Sun *et al* 2013 where a more sophisticated but computationally expensive green roof component of PUCM was validated in great detail; this component is not used here). When coupled into WRF, PUCM can be also used to evaluate the city-scale impacts of these mitigation strategies, i.e. the feedback of these strategies on atmospheric properties over the whole city, which then feedback to influence building-scale impacts.

Different combinations of PBL schemes and thermal roughness length (z_{0T}) parameterizations are tested (details in section 2.3) due to the significant sensitivities of WRF-simulated surface and air temperatures to these schemes/parameterizations, as will be illustrated later in section 3.1. Some physical parameterization schemes that were selected and not changed include: (1) the rapid radiative transfer model scheme for longwave radiation; (2) the Dudhia scheme for shortwave radiation; (3) the 2D Smagorinsky scheme for horizontal mixing; (4) the Noah land surface model for non-urban surfaces.

The WRF simulations are performed over the Baltimore–Washington metropolitan area using three nested domains with horizontal grid resolutions of 9 km, 3 km and 1 km. Cumulus parameterization was not used for any of the domains since even the largest grid size is less than 10 km and there is no rainfall during the simulation period. One-way nesting is used since all the analyses are conducted using the highest-resolution results from the innermost domain (d03, see figure 1). The domain configuration and the land-use map are shown in figure 1. The largest domain (d01) covers most of the northeastern US; d02 includes Delaware, most of Maryland and parts of West Virginia and Virginia; d03 covers the Baltimore–Washington metropolitan area. The Baltimore–Washington metropolitan area is treated as a whole because previous studies have found that the upwind UHI effect in Washington area can have a significant impact on the downwind meteorology in the Baltimore area (Zhang *et al* 2011). The three domains have 100, 100 and 121 horizontal grid cells, respectively, in both x (East–West) and y (North–South) directions. In the vertical direction, 109 levels are used to resolve the bulk boundary layer structure. All simulations start from 0000UTC on 9 June and end at 0000UTC on 10 June 2008, with a duration of 24 h and an output frequency of 10 min. We also conducted one simulation (case 6 in table 1) that is initialized at 0000UTC on 6 June, and the validation results shown in section 3 are not very different between the two simulations with different initial conditions. Hence for validation purposes in this paper, the simulation period is chosen to be from 0000UTC 9 June to 0000UTC 10 June 2008. However, we note that in the companion paper that examines the effectiveness of different mitigation strategies, the simulations span from 0000UTC 6 June to 1200UTC 10 June 2008 (Li *et al* 2014) since there we introduce cool and green roofs that alter the urban microclimate and a warm-up period is thus needed to reduce the effect of initialization from data where such roofs are absent. The initial and boundary conditions for the WRF simulations are taken from the North American Regional Reanalysis (NARR; details can be found on http://emc.ncep.noaa.gov/mmb/rreanl/ and on http://rda.ucar.edu/datasets/ds608.0/). The land-use map is taken from the National Land Cover Data (NLCD) 2006 (Fry *et al* 2011). As can be seen in figure 1, the three urban categories (i.e., low density residential, high density residential, and industrial/commercial) that are needed by the UCM can be distinguished in NLCD2006.

2.2. WRF computations of urban and rural temperatures

In our study, the UHI is defined as the difference between urban and rural temperatures. Two different UHI indices are usually used in the literature, one based on surface temperature, and the other based on near-surface air temperature at 2 m (Voogt and Oke 2003). Air temperature at 2 m can directly influence human comfort, while surface temperature contributes to the radiative component of thermal comfort and to the surface heat fluxes that produce higher air temperatures. As such, both the surface temperature and 2 m air temperature affect human comfort, and higher surface and 2 m air temperatures are often associated with higher mortality risks during heat waves (Anderson and Bell 2011). Both can also significantly affect urban energy and water consumptions (Akbari *et al* 2001). As such, both UHI indices are considered in this study and in the companion study that examines the city-scale impacts of UHI mitigation strategies. Here, the detailed calculations of surface temperature and 2 m air temperature in WRF–UCM are presented since they impact the validation and interpretation of the results.

2.2.1. Non-urban grid cells. Surface temperature (T_s) in WRF is a prognostic variable that is calculated to close the surface energy balance:

$$R_n = H + LE + G, \tag{1}$$

where R_n is the net radiation, H is the sensible heat flux that heats the urban air, LE is the latent heat flux resulting from evapotranspiration, and G is the ground heat flux. All variables are functions of surface temperature (Chen and Dudhia 2001) and are in units of W m^{-2}. In particular, the sensible heat flux H is calculated through:

$$H = \rho C_h U \left(T_s - T_a\right), \tag{2a}$$

where ρ is the air density (kg m^{-3}); C_h is the transfer coefficient that corresponds to the first level of the atmospheric model (Brutsaert 2005); and U is the wind speed at the first level of the atmospheric model. T_s is the surface temperature and T_a is the air temperature at the first level of the atmospheric model.

2 m air temperature (T_2) is a diagnostic variable that is calculated based on the alternative expression of the sensible

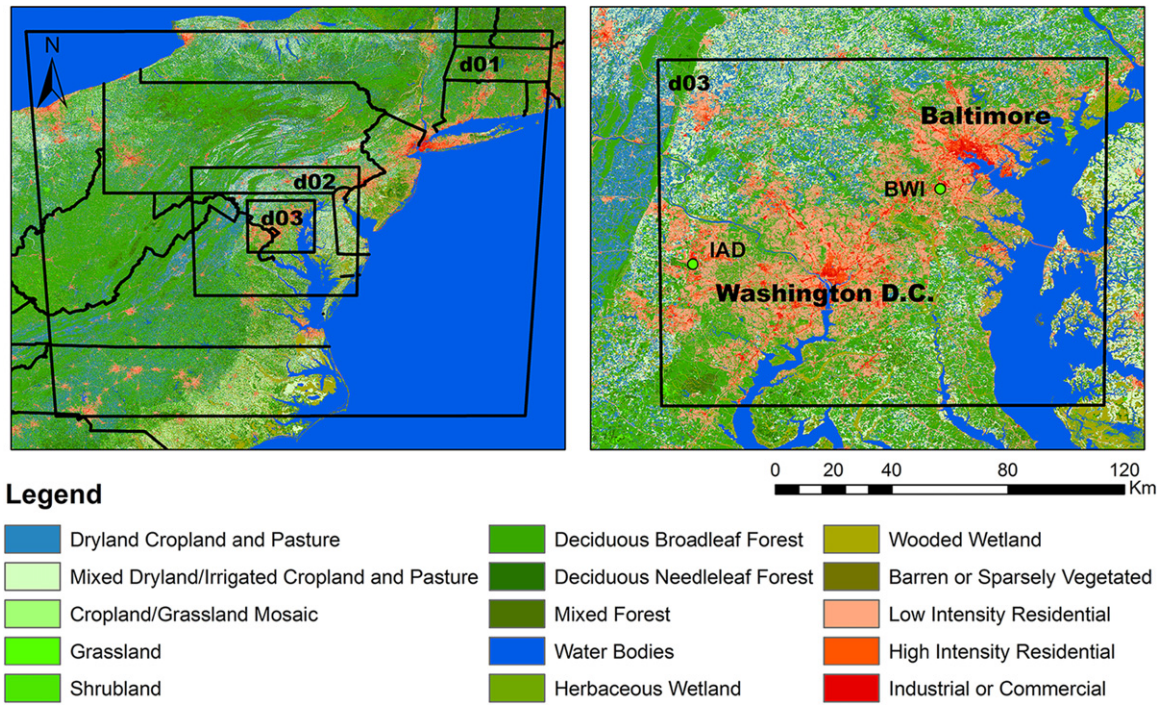

Figure 1. WRF set-up and land use/land cover maps over the Baltimore–Washington Corridor.

Table 1. Basic configuration of the WRF simulations.

Simulation number	PBL schemes	z_{0T} parameterizations	UCM
1	YSU	MM5	Default UCM
2	MYJ	Zilitinkevich	Default UCM
3	YSU	CZ09	Default UCM
4	MYJ	CZ09	Default UCM
5	MYJ	CZ09	No UCM
6	MYJ	CZ09	PUCM
7	MYJ	CZ09	Default UCM with calibrated properties

heat flux that uses atmospheric variables at 2 m:

$$H = \rho C_{h2} U_2 \left(T_s - T_2\right), \tag{2b}$$

where C_{h2} is the transfer coefficient at 2 m; U_2 is the wind speed at 2 m; and T_2 is the air temperature at 2 m. As such, T_2 can be calculated as:

$$T_2 = T_s - \frac{H}{\rho C_{h2} U_2}, \tag{3}$$

where H is the same flux computed by WRF through equation (2a). The transfer coefficients C_h and C_{h2} are calculated using the Monin–Obukhov Similarity Theory (Monin and Obukhov 1954):

$$C_h = \frac{\kappa^2}{\left[\ln\left(\frac{z}{z_0}\right) - \psi_m\left(\frac{z}{L}\right)\right]\left[\ln\left(\frac{z}{z_{0T}}\right) - \psi_h\left(\frac{z}{L}\right)\right]}, \tag{4a}$$

$$C_{h2} = \frac{\kappa^2}{\left[\ln\left(\frac{2}{z_0}\right) - \psi_m\left(\frac{2}{L}\right)\right]\left[\ln\left(\frac{2}{z_{0T}}\right) - \psi_h\left(\frac{2}{L}\right)\right]}, \tag{4b}$$

where κ (=0.40) is the von Kármán constant; z is the height of the first grid level of the atmospheric model (m); z_0 is the momentum roughness length (m); z_{0T} is the thermal roughness length (m); and L is the Obukhov length scale (m). ψ_m and ψ_h are the stability correction functions for momentum and heat, respectively (Brutsaert 1982).

From equations (2)–(4), it is evident that the momentum roughness length (z_0) and the thermal roughness length (z_{0T}) can have a significant impact on the calculation of surface temperature and 2 m air temperature. The momentum roughness length (z_0) in WRF is a function of land use categories only; these categories are specified before the WRF simulations start and remain unchanged throughout the simulation. Starting with version 3.2 of WRF, the momentum roughness length (z_0) can change with the seasonal changes in vegetation, but for short simulations like the ones conducted in our study, the changes in the momentum roughness length are negligible. The thermal roughness length (z_{0T}) in WRF, on the other hand, depends on a variety of physical factors that change significantly with time. Some of the parameterizations for the thermal roughness length that are available in WRF are listed in table 1.

The Yonsei University (YSU) PBL and surface scheme has a default parameterization for the thermal roughness length that is based on Carlson and Boland (1978, hereafter MM5 due to its use in the Penn State-NCAR fifth-generation Mesoscale Model). The thermal roughness length for that

scheme is calculated as (Chen and Dudhia 2001):

$$z_{0T} = \frac{1}{\frac{\kappa u_*}{k_a} + \frac{1}{z_l}}, \quad (5a)$$

where k_a is the molecular thermal diffusivity of air (taken in WRF to be 2.4×10^{-5} m^2 s^{-1}, i.e. at an air temperature of about 0 °C); u_* is the friction velocity; and $\kappa u_* / k_a$ represents the thermal roughness length of a hydrodynamically smooth surface. z_l (=0.01 m) is conceived as the height above which only the turbulent heat transfer mechanism is important, while molecular/radiative heat transfer mechanisms are not important (Carlson and Boland 1978). z_l is intended to represent the increase in thermal exchanges and in thermal roughness length when the surface is hydrodynamically rough, but given the default values used in WRF, its contribution is very minor.

The Mellor–Yamada–Janjic (MYJ) PBL and surface scheme has a default parameterization for the thermal roughness length that is based on Zilitinkevich's (1995, hereafter 'original Zilitinkevich') formulation:

$$z_{0T} = z_0 e^{-\kappa C_{zil}\sqrt{\mathrm{Re}}}, \quad (5b)$$

where $Re = z_0\, u_*/\nu$ is the roughness Reynolds number, ν the kinematic viscosity of air, and C_{zil} is an empirical coefficient that, in the original formulation, is set to be 0.1 based on field measurements over grassland (Chen *et al* 1997).

Later, Chen and Zhang (2009) provided a parameterization for C_{zil} in the Zilitinkevich relationship, as follows:

$$C_{zil} = 10^{-0.4h}, \quad (5c)$$

where h is the height of the canopy (m). As such, C_{zil} is no longer treated as a constant. Chen and Zhang (2009) have shown that for tall canopies ($h > 2.5$ m), C_{zil} is smaller than the 0.1 value used in the original Zilitinkevich relationship. As a result, z_{0T} is enhanced and the transfer coefficient C_h is increased in comparison to the original Zilitinkevich relationship for tall canopies, which can result in a reduction in the modeled surface temperature. The opposite situation is true for short canopies ($h < 2.5$ m). This 'modified Zilitinkevich' relationship (combining equations (5b) and (5c), hereafter CZ09) can also be used with the YSU PBL scheme in lieu of equation (5a) if the user explicitly specifies these choices (recall that the default z_{0T} for YSU PBL scheme is given by equation (5a)).

2.2.2. Urban grid cells. Any grid cell whose dominant land use category is one of the three urban categories (i.e., low density residential, high density residential, and industrial/commercial) will be treated as an urban grid cell (WRF uses only the dominant land-use in each cell). When no UCM is used, the surface temperature and 2 m air temperature in urban grid cells are calculated in the same way as described in section 2.2.1 for non-urban surfaces, but using urban-specific values of z_0 and hence of z_{0T}. When a UCM is used, any urban grid cell is first divided into two parts: an impervious part and a vegetated part consisting of grass-covered soils (see figure 1 of the companion paper). The assigned fractions of the urban and vegetated parts depend on which of the three urban categories is the dominant land use category in this grid cell. For an urban grid cell that is dominated by low density residential, 50% of the grid cell is composed of impervious surfaces. For urban grid cells that are dominated by high density residential and industrial/commercial, 90% and 95% of the grid cell surface will be treated as impervious, respectively (Chen *et al* 2011). The remainder is the vegetated surface fraction. These are the default fractions used in WRF that we do not alter here. The Noah land surface model will be called first to calculate the surface temperature for the vegetated part, and then an UCM will be called to calculated the surface temperature for the impervious part.

The surface temperature for an urban grid cell in this study is computed as a weighted average that depends on the surface temperatures of the impervious part ($T_{s(\mathrm{impervious})}$) and the vegetated part ($T_{s(\mathrm{vegetated})}$):

$$T_s = f_{impervious} \times T_{s(\mathrm{impervious})} + \left(1 - f_{\mathrm{impervious}}\right) \times T_{s(\mathrm{vegetated})}, \quad (6)$$

where $f_{\mathrm{impervious}}$ is the impervious surface fraction. The vegetated surface temperature is calculated following the methods detailed in section 2.2.1 by the Noah land surface model using the properties of grasslands. Then, the impervious surface temperature in the default WRF implementation is generated as a diagnostic variable by the UCM following:

$$T_{s_{(impervious)}} = T_a + \frac{H_{\mathrm{impervious}}}{\rho C_h U}, \quad (7)$$

where the sensible heat flux $H_{\mathrm{impervious}}$ is an area-weighted average of sensible heat fluxes from the different roof and the canyon facets ($=f_{roof} H_r + \left(1 - f_{roof}\right) H_c$, where f_{roof} is the roof fraction of the impervious surface, H_r and H_c are sensible heat fluxes from the roof and canyon, respectively). Equation (7) for calculating the impervious surface temperature is correct only if the turbulent transfer coefficient C_h is using representative momentum and thermal roughness lengths for the impervious surfaces. Nonetheless, this is not the case in WRF. In the WRF version used in this study, the turbulent transfer coefficient C_h for the whole urban grid is inaccurately calculated using the momentum and thermal roughness lengths of the vegetated grassland urban surfaces. This inconsistency will lead to large biases in simulated urban surface temperatures that we will depict, and remove, later in the paper (see figure 5 and discussions afterwards). The 2 m temperature for an urban grid cell is then calculated as in equation (3), but using the grid cell-averaged surface temperature and the grid-cell averaged sensible heat flux following:

$$T_2 = T_s - \frac{f_{impervious} \times H_{\mathrm{impervious}} + \left(1 - f_{\mathrm{impervious}}\right) \times H_{vegetated}}{\rho C_{h2} U_2}, \quad (8)$$

where T_s is given by equation (6); C_{h2} is the value of the

turbulent transfer coefficient over grass at 2 m. While one could use the transfer coefficient over the impervious patch or an effective/average one for this computation, we will continue to use this default T_2 computation method included in WRF for urban areas (this is especially relevant for the companion paper dealing with mitigation strategies). The reasons for this choice is that the 2 m air temperature is much less sensitive to the value of C_{h2} than the surface temperature, and in WRF this is simply a diagnostic representative near-surface urban air temperature that does not truly represent the air temperature at an elevation of 2 m given the complexity of the urban surface. It is thus a good diagnostic variable that would capture the bulk influence of mitigation strategies on air temperatures in cities.

2.3. Numerical experiments design

The surface and 2 m temperatures are strongly affected by the PBL schemes and the thermal roughness length parameterizations adopted in WRF. In this study, as mentioned before, different combinations of PBL schemes (i.e., the YSU and MYJ schemes) and thermal roughness length parameterizations (MM5, Zilitinkevich, and CZ09) are tested. The WRF-simulated urban surface temperature and 2 m air temperature are also sensitive to the adopted UCM. As such, the experiments are designed to intercompare the sensitivity of WRF-simulated UHIs to different combinations of PBL schemes, thermal roughness length parameterizations, as well as the use of different UCMs. The two different PBL schemes described above are both tested, each with its default z_{0T} parameterization (cases 1 and 2). We also use the modified Zilitinkevich relationship (CZ09) together with both PBL schemes (cases 3 and 4) in order to assess the relative influence of PBL schemes and the z_{0T} parameterizations on the simulated UHI. The default UCM is used for these four simulations. Three additional simulations are conducted to assess the performance of different UCMs in simulating the urban temperatures. Case 5 does not use a UCM and case 6 uses the PUCM, which was described in section 2.1. In this study, the roof component of the PUCM is composed exclusively of conventional roofs. The ground component includes asphalt, concrete, and urban grass whose fractions are 50%, 30% and 20%, respectively (Wang *et al* 2013). Case 7 uses the default UCM but with the calibrated surface properties that are used in the PUCM (Wang *et al* 2013). Note that the default UCM only has one facet over the ground-level canyon surface, which is treated as an impervious surface. As such, the surface properties used in case 7 are weighted-averages of the properties of concrete and asphalt (the two impervious surface materials) used in case 6, assuming the same ratio of concrete to asphalt surface fractions as in case 6 (i.e., 5 : 3). The roof properties used in case 7 are equivalent to the properties for roofs in case 6 since both are assumed to be conventional roofs. The difference between case 6 and case 7 lies in the fact that case 6 simulates the surface heterogeneity over the ground in urban environments (including concrete and asphalt as well as in-canyon urban grass which is not included in simulation 7), and in the use of an equivalent homogeneous impervious ground facet in case 7.

2.4. Experimental data sets

In order to assess the quality and reliability of WRF simulations of the UHI, observational data sets that span a large area are needed. The Moderate Resolution Imaging Spectroradiometer (MODIS) satellite observations provide a useful tool for diagnosing the biases in the WRF simulated surface UHI. The MODIS product used in our study is the MYD11A1 version-5 level-3 Land Surface Temperature (LST) product, which is available twice a day, once during daytime and once during nighttime, at a spatial resolution of 1 km. Note that the resolution of MODIS matches the resolution of our WRF simulations in domain 3. In this study, we use the daytime surface temperature measured around 1255 local standard time due to the good data quality (low cloudiness) and to the insensitivity of this parameter to model initial conditions.

The WRF-simulated boundary layer temperature profiles are also validated by comparing to measurements through commercial aircraft observations from the Aircraft Communications Addressing and Reporting System (ACARS). The ACARS data is available at the Dulles International Airport (IAD, see figure 1) and the Baltimore/Washington International Airport (BWI, see figure 1). The ACARS date set has multiple observations each day but the frequency is determined by the number of flights with installed meteorological instruments. To compare the WRF simulations to the ACARS observations, both WRF outputs and ACARS observations are interpolated to hourly intervals and 100 m vertical intervals.

3. Results

3.1. Surface UHI effect using existing WRF parameterizations

Figure 2 depicts the maps of surface temperatures from MODIS and from WRF simulations 1 to 5. As can be seen from figure 2(a), the remotely-sensed LSTs are evidently higher in the two urban areas (i.e., Baltimore and Washington D.C.) and their suburbs compared to rural surface temperatures. The surface UHI effect ranges from 5 °C to 15 °C and varies spatially. Without a UCM (figure 2(b)), the WRF-simulated LST cannot capture the distinct urban–suburban–rural contrasts that are observed in MODIS maps. With a UCM (figures 2(c)–(f)), the simulated LST patterns show a strong UHI effect along the Baltimore–Washington Corridor that is in better agreement with MODIS observations. It is clear that the simulated UHI depends significantly on the PBL schemes and the thermal roughness length parameterizations, which are the only two parameters that vary in figures 2(c)–(f). The YSU PBL scheme (figure 2(c)), with the default parameterization for thermal roughness length, produces the largest warm bias compared to MODIS observations (figure 2(a)). The bias is reduced by switching to the MYJ PBL scheme with its original Zilitinkevich

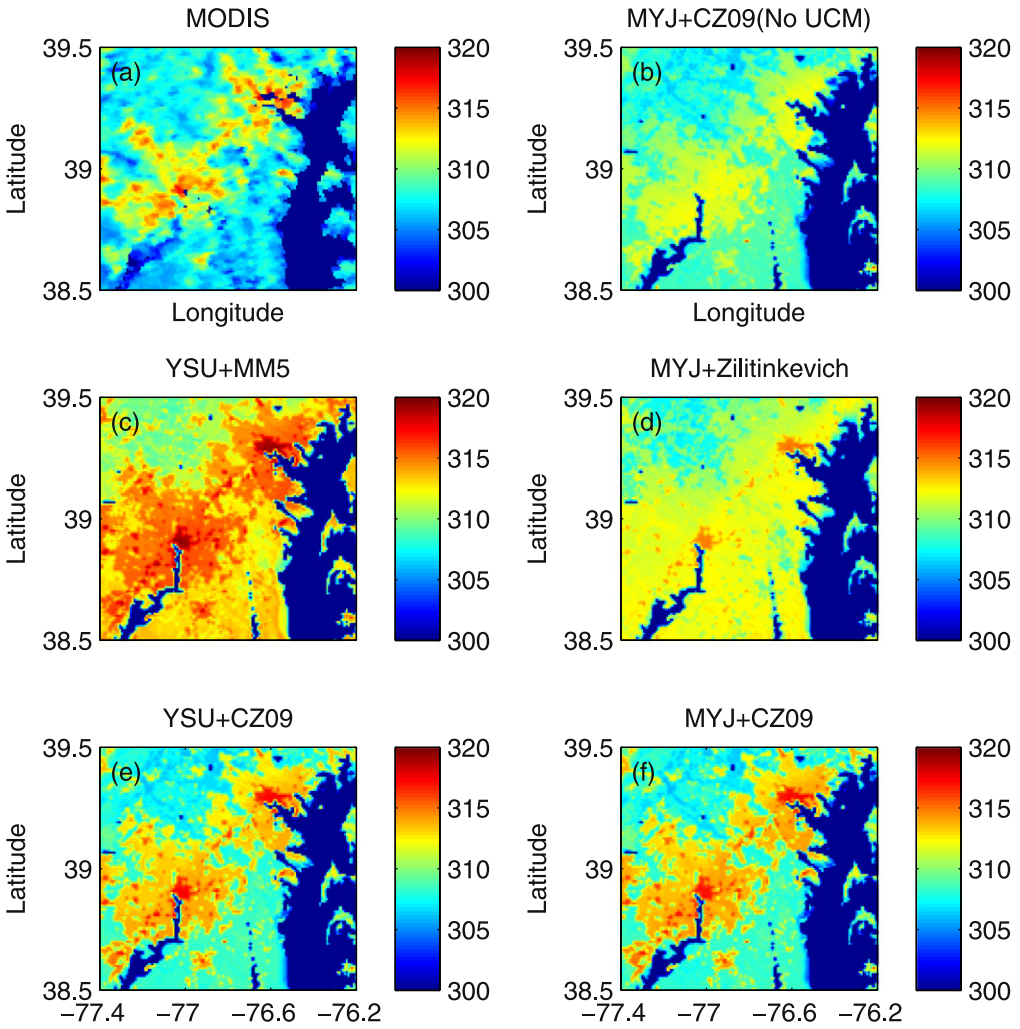

Figure 2. Land surface temperatures on 9 June 2008 at 1255PM local standard time from (a) MODIS and (b–f) WRF simulations. (b) is case 5 in table 1. (c–f) correspond to cases 1–4 (which use the default WRF UCM) in table 1, respectively (units: K).

parameterization for thermal roughness length (figure 2(d)). When the modified Zilitinkevich relationship is used with the two PBL schemes (figures 2(e), (f)), the simulated LSTs are very similar, implying that the LST at this particular time is controlled by the parameterizations for thermal roughness length, rather than by the PBL scheme. One can also clearly note that the modified Zilitinkevich relationship yields the closest agreement with MODIS, but large warm biases persist in suburban areas.

To further examine the biases in the LSTs, the differences between the WRF simulations and the MODIS observations were analyzed as a function of major land use categories within the domain (see figure 3; the categories are ordered by increasing fractions in the domains from left to right in the figure). It is again evident that the YSU PBL scheme with the MM5 parameterization for thermal roughness length yields the largest biases across all land cover types, which is consistent with figure 2(c). With the MYJ scheme and the Zilitinkevich relationship for parameterizing thermal roughness length, the biases over non-forest land cover types are significantly reduced (as can be also seen from figure 2(d)). Nevertheless, over evergreen broadleaf forest, herbaceous wetland, wooded wetland and deciduous broadleaf forest (tall canopies), the LSTs from WRF are still significantly higher than in the observations. The larger surface temperatures over these categories are caused by the fact that the original Zilintinkevich relationship underestimates the turbulent transfer coefficient C_h and thus provides an insufficient land–atmosphere coupling (and hence insufficient surface cooling) for tall canopy. As a result, the LSTs over these land use categories are significantly biased towards higher values when the original Zilintinkevich relationship is used. This is in agreement with the study of Chen and Zhang (2009), which compared the modeled transfer coefficient C_h to the calculated transfer coefficient using measurements of sensible heat flux, wind speed, air temperature and surface temperature inferred from outgoing longwave radiation. Chen and Zhang (2009) also pointed out that the transfer coefficient over tall canopy vegetation is significantly underestimated when the original Zilintinkevich relationship is used and thus provides insufficient coupling between the land surface and the atmosphere.

To resolve the problem of insufficient coupling over tall canopies, the empirical coefficient ($C_{zil} = 0.1$, see equation

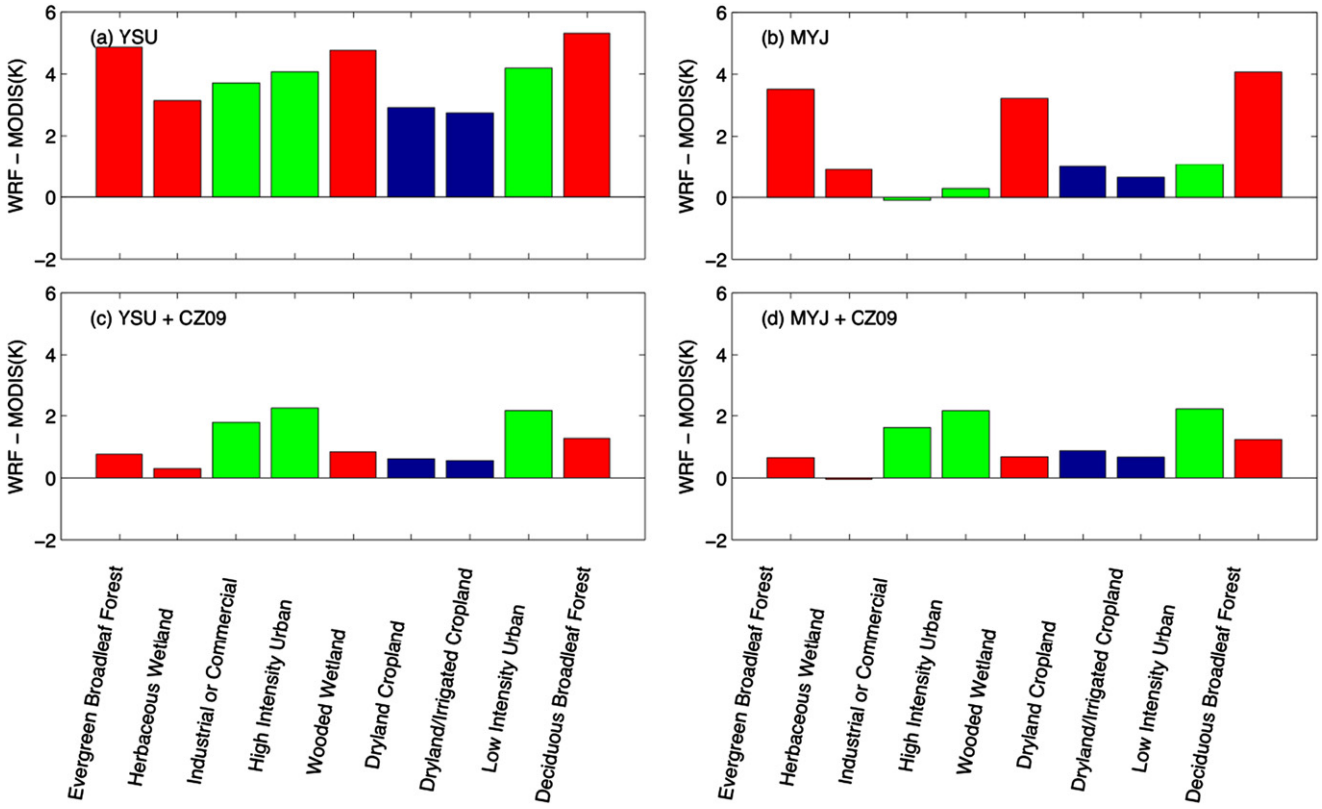

Figure 3. Land surface temperature biases on 2008-06-09 at 1255PM between WRF simulated results and MODIS observations as a function of land use categories. The sensitivities to PBL schemes and parameterizations for thermal roughness length are shown. The red color denotes tall canopy land use categories, while the blue denotes short canopy land use categories. The urban categories are in green. (a)–(d) correspond to cases 1–4 in table 1, respectively.

(5b)) used in the original Zilintinkevich relationship is modified by Chen and Zhang (2009) (see equation (5c)). This modified Zilintinkevich relationship strengthens land–atmosphere coupling over tall canopies such as evergreen broadleaf forest, herbaceous wetland, wooded wetland and deciduous broadleaf forest; this reduces the modeled surface temperatures, as well as the biases (compare figures 2(e) and (f) to (d) and compare figures 3(c) and (d) to (b)). Over land cover types whose canopy heights are close to 2.5 m (such as dryland cropland or dryland/irrigated cropland whose canopy heights are about 2.1 m, see the blue in figure 3), the modeled surface temperatures are not significantly altered. Therefore, the total bias observed in the surface temperature field is reduced when using the modified Zilintinkevich relationship (i.e., the CZ09 parameterization, see equation (5c)), as compared to using the original Zilitinkevich relationship.

One notable exception to the success of the modified Zilintinkevich relationship is that in urban areas, which could also be viewed as tall canopies, the biases are increased (see the green in figure 3); this is not consistent with the reasoning and results for tall vegetated canopies (cf figures 3(b)–(d)). Close scrutiny however reveals that this bias is linked to the use of the vegetated transfer coefficient to infer/compute the diagnostic averaged urban surface temperatures as detailed after equation (7). When a UCM is used, each urban grid will be assigned a certain fraction of vegetated surface (grassland), with the remainder being the imperious surface. The Noah land surface model will be called first to calculate the surface temperature for the vegetated part, and then the UCM will be called to calculated the surface temperature for the impervious part. After the Noah land surface model calculates the vegetated surface temperature, the transfer coefficient C_h calculated over the vegetated surface is used by WRF to compute an impervious surface temperature using equation (7) (i.e., the turbulent transfer coefficient C_h is computed using the momentum and thermal roughness lengths of grasslands rather than buildings). Over short canopy vegetation types like grassland, the turbulent transfer coefficient C_h is reduced when the modified Zilitinkevich relationship is used, which increases the modeled surface temperature (compared to the original Zilitinkevich). This explains the larger warm biases in the modeled LST over urban areas when the modified Zilitinkevich relationship is used (cf figures 3(b)–(d)). This large bias in the urban surface temperature field can be corrected by the use of a more accurate computation of the impervious surface temperature, and an improved UCM, as will be discussed in section 3.2.

To further investigate the sensitivity of LSTs to PBL schemes and to parameterizations for the thermal roughness length, figure 4 depicts the diurnal cycles of surface temperature averaged over all rural (figure 4(a)) and urban (figure 4(b)) grids produced with different PBL schemes and thermal

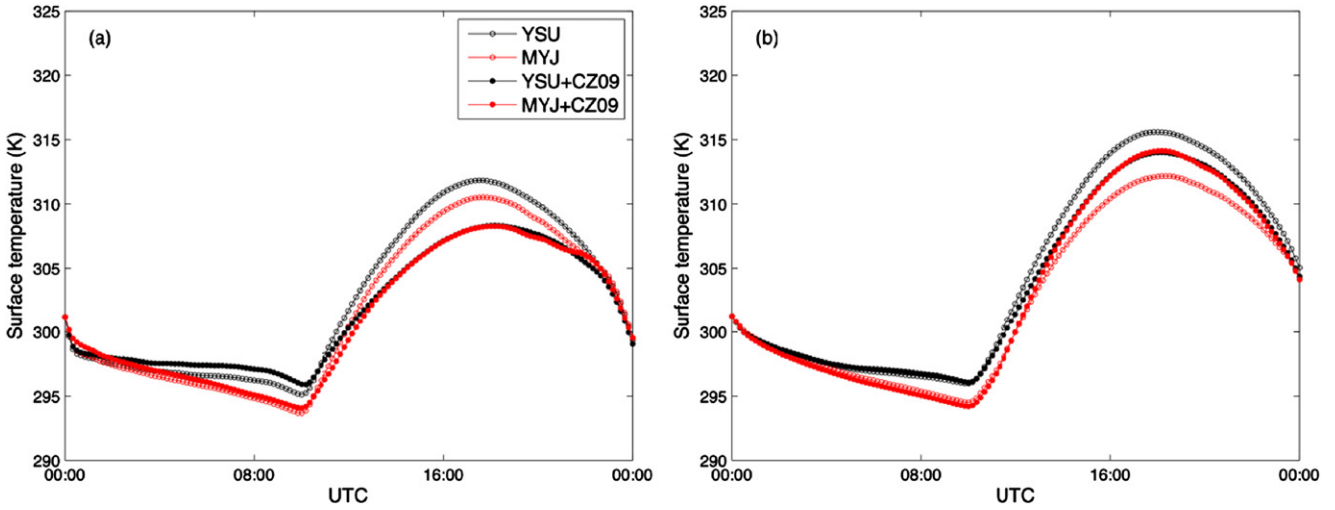

Figure 4. Diurnal cycles of spatially averaged (a) rural and (b) urban surface temperatures in domain 3 produced by the WRF–UCM with different PBL schemes and thermal roughness length configurations.

roughness length parameterizations. The urban grids include those whose dominant land use category is one of the three urban categories; all other grid cells are considered rural (except those dominated by open water bodies). During daytime, the surface temperature is clearly more sensitive to the parameterization of the thermal roughness length than to the PBL scheme, as one can see from both panels in figure 4 where the daytime results with the same parameterization for z_{0T} (the CZ09) match very well, regardless of the PBL scheme. This is consistent with the comparison in figure 2 that showed snapshots of surface temperature around 1255PM. During nighttime, however, the surface temperature is more sensitive to the PBL scheme compared to the parameterization of z_{0T}. Changing parameterizations for thermal roughness length does not alter the surface temperature significantly during the night, when the turbulent fluxes are weak and the surface energy budget is dominated by the radiative terms. The results with the same PBL scheme thus match well, while those with different PBL schemes diverge. The larger sensitivity of WRF-simulated surface temperature to z_{0T} during daytime is in agreement with many previous studies that also used WRF or other numerical models. For example, Zeng *et al* (2012) show that changing the coefficients in computing the thermal roughness length (similar to the coefficient in the Zilitinkevich relationship that is examined in our study) significantly alters the daytime surface temperature but has a negligible effect on nighttime surface temperature over arid areas. Zheng *et al* (2012) also demonstrate that the simulated daytime surface temperature can be improved by improving the thermal roughness length parameterization. Shin and Hong (2011) found that when the PBL scheme is fixed in WRF, switching the surface-layer formulations (and thus changing parameterizations for the thermal roughness length) has an important impact on the simulated daytime surface temperature; nevertheless, it does not significantly alter the nighttime surface temperature (see their figure 9(a)).

Figure 4(a) also illustrates that when the CZ09 relationship is used in the parameterization for thermal roughness length (comparing MYJ + CZ09 to MYJ), the daytime rural surface temperature is reduced and hence the biases (compared to MODIS) are reduced. This is again due to the fact that most of the rural land-use categories in our domain have tall canopies. In addition, the only two categories that are not classified as tall canopy land-uses (dryland cropland and dryland/irrigated cropland) also have canopy heights that are fairly close to 2.5 m, which is the criterion to separate tall canopies from short canopies. On the other hand, comparing MYJ + CZ09 to MYJ over urban terrain (figure 4(b)), one notes that the daytime urban surface temperature is increased and hence the biases are increased, which, as discussed before, is caused by the erroneous use of C_h calculated over grassland for impervious surfaces.

3.2. Improving the WRF-simulated surface UHI effect

In order to reduce the biases observed in urban surface temperatures when MYJ + CZ09 are used, and to overcome the inconsistency of using the turbulent transfer coefficient (C_h) calculated over grassland for impervious surfaces, the calculation of impervious surface temperature in the UCM is revised. Given that the UCM combines fluxes from the roof and the canyon (see discussion after equation (7)), in the following analyses, the prognostically-computed temperatures of the roof surface and the canyon are aggregated to yield an average surface temperature over the impervious surface, following

$$T_{s(impervious)} = f_{roof} \times T_r + \left(1 - f_{roof}\right) \times T_c. \qquad (9)$$

This is similar to the 'complete urban surface temperature' concept proposed by Voogt and Oke (1997), but the wall and ground temperatures are incorporated into the 'complete urban surface temperature' through the canyon temperature T_c. Note that the T_c given by the UCM is not the air temperature in the canyon. It is rather an equivalent aerodynamic surface temperature aggregated for canyon surfaces (walls and ground). This is because

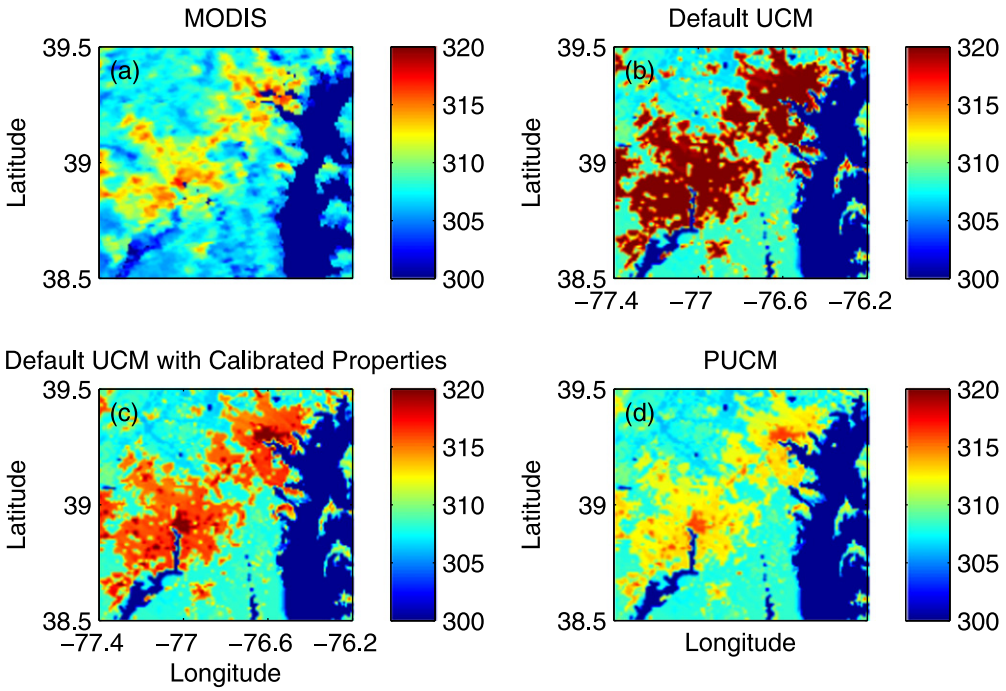

Figure 5. Similar to figure 2; land surface temperature (units: K) on 9 June 2008 at about 1255PM local standard time measured by (a) MODIS and produced by (b–d) WRF. (b) Is with the default UCM and default thermal properties, (c) is with default UCM and calibrated properties, and (d) is with the PUCM and calibrated properties. All of these simulations use the MYJ scheme and the CZ09 parameterization for z_{0T}. In urban grids, the impervious surface temperature is a weighted average of roof temperature and canyon temperature (equation (9)).

$H_c = \rho C_{hc} U \left(T_c - T_a\right) = \left(2h/Rd\right) H_w + H_g$, where h is the building height and Rd is the road width; $H_w = \rho C_{hw} U \left(T_w - T_c\right)$ and $H_g = \rho C_{hg} U \left(T_g - T_c\right)$. As such, the canyon temperature can be calculated as:

$$T_c = \frac{\left(2h/Rd\right) C_{hw} T_w + C_{hg} T_g + C_{hc} T_a}{\left(2h/Rd\right) C_{hw} + C_{hg} + C_{hc}}. \quad (10)$$

Note that the subscripts 'r', 'w', 'g', 'c', 'a' denote roof, wall, ground, canyon and air, respectively. This justifies the use of the canyon temperature as an effective surface temperature for the canyon. The impervious surface temperature calculated using equation (9) is then substituted into equation (6) in order to obtain a surface temperature that represents the whole urban grid cell. Using this approach, the calculated surface temperature patterns from equation (6) for the default UCM, the default UCM with calibrated properties, and the PUCM are compared to the MODIS satellite observations in figure 5. As can be seen in figure 5(b), the surface temperatures calculated using this method and the default UCM are substantially larger than the MODIS observations, implying that this default UCM (including the surface properties used in this default UCM) are very deficient in simulating surface UHI strengths. The simulation with the PUCM (figure 5(d)) on the other hand clearly gives the best estimate of land surface temperatures for the whole region when compared to the MODIS observations. The PUCM includes 'urban grass' on the ground and the properties of each facet were calibrated at a site in the Northeastern US (Princeton, NJ) using a wireless sensor network (Wang *et al* 2013). Note that the green roof fraction is set to zero so that, effectively, the roof still has only one surface type. To separate the impact of introducing urban grass into the UCM and the impact of modified facet properties, as mentioned earlier, we also modified the properties of the default UCM so that it uses the properties of the non-vegetated facets that are used in the PUCM (figure 5(c)). In this case, the roof, wall, and ground material properties are modified, but the ground surfaces are still completely impervious (consisting of asphalt and concrete pavements). Using the default UCM with calibrated properties reduces the bias considerably compared to the default UCM with default properties, but it still yields a relatively larger bias compared to the PUCM, which implies that inclusion of urban grassland (inside the canyon) is crucial for reproducing the correct urban surface features. The difference is particularly significant in suburban areas where the presence of in-canyon vegetation, is important but not captured by the default UCM.

We again quantify the biases in the LSTs as a function of the three urban categories for these runs in table 2. Here, the No-UCM simulation (case 5) is added as a reference. It is interesting to see that the No-UCM case does not produce the largest biases in the urban surface temperatures, despite its erroneous simulation of the spatial patterns of the UHI (figure 2(b)). However, since the simulated LSTs for the three urban categories are not significantly different with this option for the three urban categories (i.e., the three urban categories have similar simulated surface temperatures), as can be seen from figure 2(b), the biases for the three urban categories are quite different. In other words, the variability in

Table 2. Surface temperature biases generated by different UCMs in the three urban categories.

	Mean biases (K)		
UCMs	Industrial or commercial urban	High density residential urban	Low density residential urban
No UCM	−2.3	−1.9	−0.03
Default UCM	10.2	11.0	7.4
Default UCM with calibrated properties	3.8	4.7	3.8
PUCM	0.4	1.0	1.1

the urban surface temperature (and in the UHI effect) is not captured by the No-UCM case. On the other hand, the other three cases produce varying biases for the three urban categories. The default UCM yields the largest biases, which can reach up to 11 K. The default UCM with the calibrated properties reduces the biases significantly, but the errors remain relatively large (4–5 K). The new PUCM clearly produces the smallest bias (<1.5 K) as compared to the MODIS observations. In addition, this bias is comparable to the uncertainty in the MODIS LST product. Inter-comparing the values in table 2 indicates that introducing urban grass into the UCM has a comparable impact on the surface temperature biases as modifying the surface properties in the default UCM. Another study by the authors (Li and Bou-Zeid 2013) includes further comparisons of WRF-simulated to MODIS-observed UHI over this area in three other days during the period from 5 June to 14 June 2008. PUCM captures the surface UHI effect in three other days during that period as well (see their figure 7), implying that our conclusion that WRF-PUCM can realistically represent the surface UHI effect over this area is robust.

3.3. Boundary-layer temperature profiles

In addition to the comparison of the modeled surface temperatures to MODIS observations, an important parameter to validate is air temperature, which is also a main determinant of thermal comfort in cities. Due to the use of C_h calculated over grassland for impervious surfaces, the 2 m air temperature calculated in urban grids might not be the most suitable temperature to validate in urban terrain (it is not clear what elevation it would actually correspond to over complex canopies), despite the fact that in the companion paper we do use this 2 m temperature as a representative air temperature for assessing the impact of mitigation options. For validation purposes, a better test is the ability of WRF to reproduce the full atmospheric boundary layer temperature fields. To verify such ability, the WRF-simulated potential temperature profiles in the lower atmosphere (from 0.1 km to 3 km) at the IAD and the BWI are compared to ACARS observations, which were introduced earlier.

The IAD site is identified as an urban site due to a large fraction of urban land within the grid cell where IAD is located. The grid cell has 81%, 14% and 5% of low-density residential urban land, high-density residential urban land, and industrial/commercial urban land, respectively. While the BWI site has 35% low-density residential urban land, it is primarily dominated by deciduous broadleaf forest (40%) and has 10% deciduous needleleaf forest.

Figure 6 illustrates the evolution of potential temperature in the lower atmosphere (up to 3 km above ground level) at IAD (left panel) and BWI (right panel). As can be seen in the figure, WRF simulations with different physical parameterizations (including PBL schemes and UCMs) display subtle differences, indicating that atmospheric temperature fields are less sensitive to these parameterizations than surface temperature fields. This is not surprising given the constraint imposed by the surface energy balance on surface-atmosphere fluxes, which reduces the sensitivity of these fluxes to PBL and surface schemes. One can note however that the afternoon temperatures obtained with PUCM at the end of the run match the observations better (cooler near surface temperatures than other models), which is related to the cooler surface temperatures produced by PUCM.

The mean potential temperature profiles over the diurnal cycle from observations and WRF simulations are shown in figure 7. Overall, the composite potential temperature profiles from the WRF simulations match the ACARS measurements better within the atmospheric boundary layer than above the atmospheric boundary layer. The biases inside the atmospheric boundary layer are on the order of 1 ~ 1.5 °C, implying that WRF simulations capture the boundary layer temperature profiles reasonably well. Changing PBL schemes and UCMs alters the temperature profiles within the atmospheric boundary layer at both IAD and BWI; and the differences between WRF runs with two PBL schemes are comparable to those between WRF runs with different UCMs. Interestingly, at both locations, the case without a UCM seems to produce the largest differences with the other cases. The case without a UCM seems to better reproduce the temperature profiles while the case with PUCM seems to yield the largest biases at BWI; however, at IAD, slightly larger biases are associated with the case without a UCM and relatively smaller biases are observed for the case with PUCM. This, along with the vertical variability of the biases, prevent us from making general conclusions about the most suitable UCM for reproducing the boundary layer temperature profiles in WRF. But what we can conclude is that WRF is able to capture the bulk structure of potential temperature in the atmospheric boundary layer realistically.

4. Conclusions and discussions

In this study, numerical simulation of the UHI effect at the city scale is investigated using a regional climate model (WRF) at high spatial resolutions. The simulated UHI with WRF is validated against remotely-sensed and *in situ* observations from aircraft mounted sensors. The results indicate

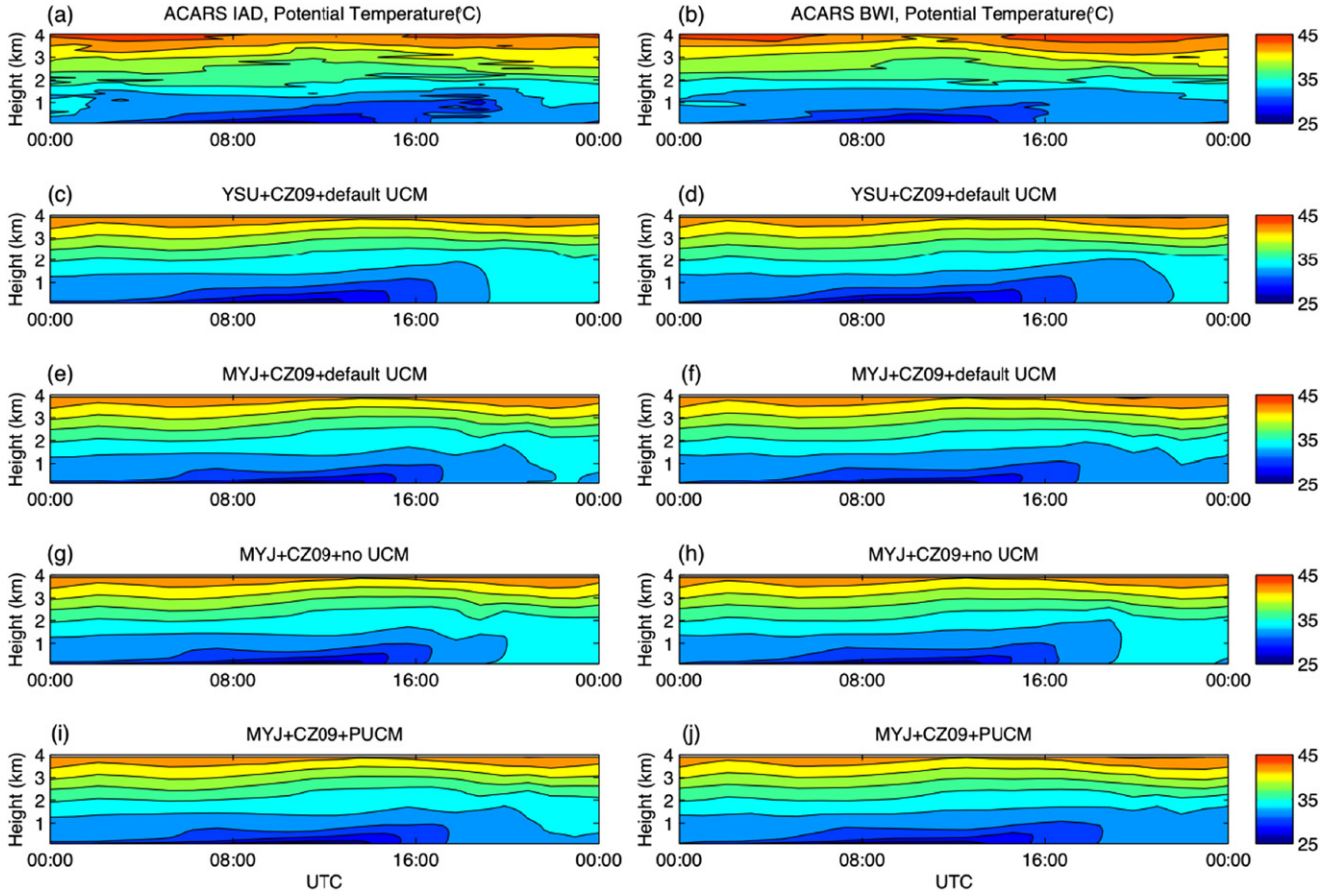

Figure 6. Evolution of potential temperature in the lower atmosphere (up to 4 km above the ground level) at the Dulles International Airport (IAD, left panels) and the Baltimore/Washington International Airport (BWI, right panels) on 9 June 2008; time is UTC and local noon is thus 1700 UTC. The top panels (a), (b) are aircraft measurements and the other panels are results with different WRF simulation ((c) and (d): YSU + CZ09 + default UCM; (e) and (f): MYJ + CZ09 + default UCM; (g) and (h): MYJ + CZ09 + No UCM; (i) and (j): MYJ + CZ09 + PUCM).

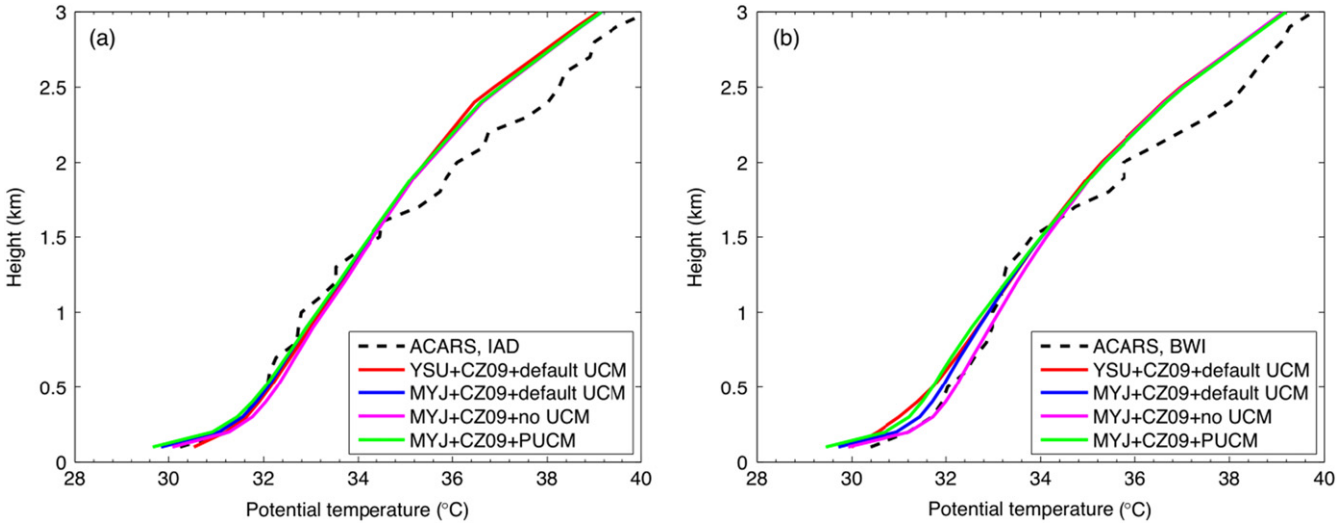

Figure 7. Composite profiles of potential temperature in the lower atmosphere (up to 3 km above ground level) at the Dulles International Airport (IAD, a) and the Baltimore/Washington International Airport (BWI, b) on 9 June 2008.

that the WRF-simulated surface temperatures are highly sensitive to both PBL schemes and the thermal roughness length parameterizations used in WRF. In particular, the surface temperatures are more sensitive to the PBL schemes during nighttime and more sensitive to the thermal roughness length parameterizations during daytime. The use of the CZ09 parameterization for thermal roughness length (a modified Zilitinkevich relationship) produces the smallest biases in the

surface temperature fields over natural surfaces when compared to satellite measurements during daytime.

The urban surface temperatures simulated by WRF are also sensitive to the UCMs used, as well as to the imposed urban thermal surface properties (e.g., albedo, thermal capacity, and thermal conductivity). A more consistent method for calculating urban surface temperature is proposed and validated in this study. Compared to not using a UCM or using the default UCM, an improved UCM (the PUCM), which we implemented into WRF, yields the smallest bias (<1.5 °C) in the urban surface temperature fields, though part of this improved performance is attributed to the use of more accurate surface thermal properties.

WRF-simulated potential temperature profiles in the atmospheric boundary layer are then compared to aircraft observations. Results show that WRF captures the boundary layer potential temperature profiles reasonably well at both the urban and the rural sites considered here. The biases are about 1.5 °C in the atmospheric boundary layer. The performance of WRF in reproducing the boundary layer structure is not very sensitive to the PBL schemes and the surface physical parameterizations such as the UCMs.

The implementation and use of PUCM not only improve the performance of WRF in reproducing the LST patterns and the associated surface UHI intensity, but also allow a realistic investigation of UHI mitigation strategies such as the green roof and white roof strategies. These mitigation strategies have been studied at building-scales (see e.g., Li *et al* 2013b; Sun *et al* 2014; Susca *et al* 2011; Takebayashi and Moriyama 2007) or global-scales (e.g., Jacobson and Ten Hoeve 2012; Oleson *et al* 2010; Akbari *et al* 2012). However, a problem of these previous global studies is the use of homogeneous urban properties (all roofs had to be white for example); in addition, less is known about the neighborhood and city-scale impacts of these mitigation strategies. Given that mitigation actions are usually organized and implemented at city scales and in stages, the WRF-PUCM modeling system implemented and validated in this study is extremely useful in providing a framework to answer questions related to the effectiveness of UHI mitigation strategies. It can thus bridge the gap between building-scale experimental/modeling work and global-scale modeling work. In the companion paper (Li *et al* 2014), we use this WRF-PUCM modeling system to study the city-scale impacts of green roof and cool (white) roof strategies, and we examine how these impacts scale as the penetration rate of their associated mitigation approaches increases.

Acknowledgement

This study was funded by the US National Science Foundation under Grant CBET-1058027 and the Princeton Environmental Institute-Science, Technology, and Environmental Policy fellowship. The authors would like to thank James A Smith, Mary-Lynn Baeck and Maofeng Liu from Princeton University and Ting Sun from Tsinghua University for their help in obtaining and processing some of the observational datasets. The simulations were performed on the supercomputing clusters of the National Center for Atmospheric Research through project P36861020.

References

Akbari H, Matthews H D and Seto D 2012 The long-term effect of increasing the albedo of urban areas *Environ. Res. Lett.* **7** 024004

Akbari H, Pomerantz M and Taha H 2001 Cool surfaces and shade trees to reduce energy use and improve air quality in urban areas *Sol. Energy* **70** 295–310

Anderson G B and Bell M L 2011 Heat waves in the United States: mortality risk during heat waves and effect modification by heat wave characteristics in 43 U.S. communities *Environ. Health Perspect.* **119** 210–8

Arnfield A J 2003 Two decades of urban climate research: a review of turbulence, exchanges of energy and water, and the urban heat island *Int. J. Climatol.* **23** 1–26

Bornstein R and Lin Q L 2000 Urban heat islands and summertime convective thunderstorms in Atlanta: three case studies *Atmos. Environ.* **34** 507–16

Brutsaert W 1982 *Evaporation into the Atmosphere: Theory, History, and Applications* (Dordrecht, Holland: Reidel)

Brutsaert W 2005 *Hydrology: an Introduction* (New York: Cambridge University Press)

Carlson T N and Boland F E 1978 Analysis of Urban-Rural canopy using a surface Heat flux temperature model *J. Appl. Meteorol.* **17** 998–1013

Chen F and Dudhia J 2001 Coupling an advanced land surface-hydrology model with the Penn State-NCAR MM5 modeling system. part I: model implementation and sensitivity *Mon. Weather Rev.* **129** 569–85

Chen F *et al* 2011 The integrated WRF/urban modelling system: development, evaluation, and applications to urban environmental problems *Int. J. Climatol.* **31** 273–88

Chen F and Zhang Y 2009 On the coupling strength between the land surface and the atmosphere: from viewpoint of surface exchange coefficients *Geophys. Res. Lett.* **36** L10404

Chen F, Janjic Z and Mitchell K 1997 Impact of atmospheric surface-layer parameterizations in the new land-surface scheme of the NCEP mesoscale Eta model *Boundary-Layer Meteorol* **85** 391–421

Chow W T L, Brennan D and Brazel A J 2012 Urban heat island research in phoenix, arizona theoretical contributions and policy applications *Bull. Am. Meteorol. Soc.* **93** 517–30

Christen A and Vogt R 2004 Energy and radiation balance of a central European city *Int. J. Climatol.* **24** 1395–421

Cleugh H A and Oke T R 1986 Suburban-rural energy-balance comparisons in summer for vancouver *B.C. Bound.-Layer Meteorol.* **36** 351–69

Dabberdt W and Davis P 1978 Determination of energetic characteristics of urban-rural surfaces in the greater St *Louis area Bound.-Layer Meteorol.* **14** 105–21

Dixon P G and Mote T L 2003 Patterns and causes of Atlanta's urban heat island-initiated precipitation *J. Appl. Meteorol.* **42** 1273–84

Fry J, Xian G, Jin S, Dewitz J, Homer C, Yang L, Barnes C, Herold N and Wickham J 2011 Completion of the 2006 national land cover database for the conterminous United States *Photogramm. Eng. Remote Sens.* **77** 858–64

Grimm N B, Faeth S H, Golubiewski N E, Redman C L, Wu J G, Bai X M and Briggs J M 2008 Global change and the ecology of cities *Science* **319** 756–60

Grimmond C S B, Oke T R and Cleugh H A 1993 The role of 'rural' in comparisons of observed suburban-rural flux differences *Exchange Processes At The Land Surface For A Range Of Space And Time Scales* (Wallingford, UK: IAHS Press) pp 165–74

Grimmond C S B *et al* 2010 The international Urban energy balance models comparison project: first results from phase 1 *J. Appl Meteorol. Clim.* **49** 1268–92

Grimmond C S B *et al* 2011 Initial results from Phase 2 of the international urban energy balance model comparison *Int. J. Climatol.* **31** 244–72

Grimmond C S B and Oke T R 1995 Comparison of heat fluxes from summertime observations in the suburbs of 4 north-american cities *J. Appl. Meteorol.* **34** 873–89

Grimmond C S B and Oke T R 1999 Heat storage in urban areas: local-scale observations and evaluation of a simple model *J. Appl. Meteorol.* **38** 922–40

Grimmond S 2007 Urbanization and global environmental change: local effects of urban warming *Geogr. J.* **173** 83–8

Grossman-Clarke S, Zehnder J A, Loridan T and Grimmond C S B 2010 Contribution of land use changes to near-surface air temperatures during recent summer extreme heat events in the phoenix metropolitan area *J. Appl. Meteorol. Clim.* **49** 1649–64

Jacobson M Z and Ten Hoeve J E 2012 Effects of Urban surfaces and white roofs on global and regional climate *J. Clim.* **25** 1028–44

Lau N C and Nath M J 2012 A model study of heat waves over north america: meteorological aspects and projections for the twenty-first century *J. Clim.* **25** 4761–84

Lee S H, Kim S W, Angevine W M, Bianco L, McKeen S A, Senff C J, Trainer M, Tucker S C and Zamora R J 2011 Evaluation of urban surface parameterizations in the WRF model using measurements during the texas air quality study 2006 field campaign *Atmos. Chem. Phys.* **11** 2127–43

Li D and Bou-Zeid E 2013 Synergistic interactions between urban heat islands and heat waves: the impact in cities is larger than the sum of its parts *J. Appl. Meteorol. Clim.* **52** 2051–64

Li D, Bou-Zeid E, Baeck M L, Jessup S and Smith J A 2013a Modeling land surface processes and heavy rainfall in urban environments: sensitivity to Urban surface representations *J. Hydrometeorol.* **14** 1098–118

Li D, Bou-Zeid E and Oppenheimer M 2014 The effectiveness of cool and green roofs as Urban heat island mitigation strategies *Environ. Res. Lett.* **9** 055002

Li H, Harvey J T, Holland T J and Kayhanian M 2013b The use of reflective and permeable pavements as a potential practice for heat island mitigation and stormwater management *Environ. Res. Lett.* **8** 015023

Loridan T and Grimmond C S B 2012 Characterization of energy flux partitioning in urban environments: links with surface seasonal properties *J. Appl. Meteorol. Clim.* **51** 219–41

Meehl G A and Tebaldi C 2004 More intense, more frequent, and longer lasting heat waves in the 21st century *Science* **305** 994–7

Miao S G, Chen F, Li Q C and Fan S Y 2011 Impacts of Urban processes and urbanization on summer precipitation: a case study of heavy rainfall in beijing on 1 august 2006 *J. Appl. Meteorol. Clim.* **50** 806–25

Monin A S and Obukhov A M 1954 Basic laws of turbulent mixing in the ground layer of the atmosphere *Akad. Nauk. SSSR, Geofiz. Inst. Tr.* **151** 163–87

Oke T R 1982 The energetic basis of the Urban heat-island *Q. J. R. Meteorol. Soc.* **108** 1–24

Oke T R, Spronken-Smith R A, Jauregui E and Grimmond C S B 1999 The energy balance of central mexico city during the dry season *Atmos. Environ.* **33** 3919–30

Oleson K W, Bonan G B and Feddema J 2010 Effects of white roofs on urban temperature in a global climate model *Geophys. Res. Lett.* **37** L03701

Peterson J T and Stoffel T L 1980 Analysis of Urban-Rural solar-radiation data from st-louis, missouri *J. Appl. Meteorol.* **19** 275–83

Robinson P J 2001 On the definition of a heat wave *J. Appl. Meteorol.* **40** 762–75

Ryu Y H and Baik J J 2012 Quantitative analysis of factors contributing to Urban heat island intensity *J. Appl. Meteorol. Clim.* **51** 842–54

Shephard J M 2005 A review of current investigations of urban-induced rainfall and recommmendations for the future *Earth Interact.* **9** 1–27

Shin H H and Hong S Y 2011 Intercomparison of planetary boundary-layer parametrizations in the wrf model for a single day from cases-99 *Bound.-Layer Meteorol.* **139** 261–81

Skamarock W C and Klemp J B 2008 A time-split nonhydrostatic atmospheric model for weather research and forecasting applications *J. Comput. Phys.* **227** 3465–85

Sun T, Bou-Zeid E and Ni G-H 2014 To irrigate or not to irrigate: analysis of green roof performance via a vertically-resolved hygrothermal model *Build. Environ.* **73** 127–37

Sun T, Bou-Zeid E, Wang Z-H, Zerba E and Ni G-H 2013 Hydrometeorological determinants of green roof performance via a vertically-resolved model for heat and water transport *Build. Environ.* **60** 211–24

Susca T, Gaffin S R and Dell'Osso G R 2011 Positive effects of vegetation: urban heat island and green roofs *Environ. Pollut.* **159** 2119–26

Takebayashi H and Moriyama M 2007 Surface heat budget on green roof and high reflection roof for mitigation of urban heat island *Build. Environ.* **42** 2971–9

Voogt J A and Oke T R 1997 Complete urban surface temperatures *J. Appl. Meteorol.* **36** 1117–32

Voogt J A and Oke T R 2003 Thermal remote sensing of urban climates *Remote Sens. Environ.* **86** 370–84

Wang Z H, Bou-Zeid E, Au S K and Smith J A 2011a Analyzing the sensitivity of WRF's single-layer Urban canopy model to parameter uncertainty using advanced monte carlo simulation *J. Appl. Meteorol. Clim.* **50** 1795–814

Wang Z H, Bou-Zeid E and Smith J A 2011b A spatially-analytical scheme for surface temperatures and conductive heat fluxes in Urban canopy models *Bound.-Layer Meteorol.* **138** 171–93

Wang Z H, Bou-Zeid E and Smith J A 2013 A coupled energy transport and hydrological model for urban canopies evaluated using a wireless sensor network *Q. J. R. Meteorol. Soc.* **139** 1643–57

Zeng X B, Wang Z and Wang A H 2012 Surface skin temperature and the interplay between sensible and ground heat fluxes over arid regions *J. Hydrometeorol.* **13** 1359–70

Zhang C L, Chen F, Miao S G, Li Q C, Xia X A and Xuan C Y 2009 Impacts of urban expansion and future green planting on summer precipitation in the Beijing metropolitan area *J. Geophys. Res. Atmos.* **114** D02116

Zhang D L, Shou Y X, Dickerson R R and Chen F 2011 Impact of upstream urbanization on the urban heat island effects along the Washington–Baltimore corridor *J. Appl. Meteorol. Clim.* **50** 2012–29

Zheng W Z, Wei H L, Wang Z, Zeng X B, Meng J, Ek M, Mitchell K and Derber J 2012 Improvement of daytime land surface skin temperature over arid regions in the NCEP GFS model and its impact on satellite data assimilation *J. Geophys Res. Atmos.* **117** D06117

Zilitinkevich S S 1995 *Air Pollution* vol. III, *Air Pollution Theory and Simulation* ed H Power *et al* (Southampton Boston: Computational Mechanics Publications) pp 53–60